Electronic Supplementary Information (ESI)

for

Iron(II)-α-Keto Acid Complexes of Tridentate Ligands on Gold Nanoparticles: Effect of Ligand Geometry and Immobilization on Their Dioxygen-Dependent Reactivity

*Abhijit Bera,[a] Debobrata Sheet,[b] and Tapan Kanti Paine[a,]**

[a]School of Chemical Sciences, Indian Association for the Cultivation of Science, 2A & 2B Raja S. C. Mullick Road, Jadavpur, Kolkata-700032, India. Email: ictkp@iacs.res.in

[b]Department of Chemistry, Presidency University, 86/1 College Street, Kolkata-700073, India.

Table S1. *Crystallographic data for* ***1c*** *and* ***1d****.*

Empirical formula	$C_{3.33}H_{4.22}Cl_{0.44}Fe_{0.22}N_{0.67}$	$C_{80}H_{88}Cl_8Fe_4N_{12}O_4$
Formula weight	81.8	1788.62
Temperature/K	99.96	109.94
Crystal system	monoclinic	Monoclinic
Space group	P21/c	P21/n
a/Å	8.655(5)	12.0433(6)
b/Å	12.892(7)	8.8000(4)
c/Å	14.631(8)	21.8652(12)
α/°	90	90
β/°	92.845(17)	105.9850(10)
γ/°	90	90
Volume/Å^3	1630.3(15)	2227.70(19)
Z	18	1
ρ_{calc}g/cm^3	1.5	1.333
μ/mm^{-1}	1.249	0.930
F(000)	760	924.0
Crystal size/mm^3	0.021 × 0.018 × 0.014	0.2 × 0.15 × 0.15
2Θ range for data collection/°	4.712 to 50.296	4.46 to 49.518
Index ranges	-10 ≤ h ≤ 10, -15 ≤ k ≤ 15, 17 ≤ l ≤ 17	-14 ≤ h ≤ 14, -10 ≤ k ≤ 10, -24 ≤ l ≤ 25
Reflections collected	12748	21576
Independent reflections	2768 [Rint = 0.0882, Rsigma = 0.0704]	3816 [Rint = 0.0377, Rsigma = 0.0264]
Data/restraints/parameters	2768/21/188	3816/0/248
Goodness-of-fit on F^2	1.077	1.050
Final R indexes [I>=2σ (I)]	R1 = 0.1055, wR2 = 0.2635	R1 = 0.0323, wR2 = 0.0734
Final R indexes [all data]	R1 = 0.1252, wR2 = 0.2780	R1 = 0.0417, wR2 = 0.0807
Largest diff. peak/hole / e Å^{-3}	1.40/-0.66	0.30/-0.80

Table S2. *Selected bond lengths (Å) and bond angles (°) for* ***1c****.*

Fe1-Cl1	2.297(3)	Fe1-Cl2	2.334(3)
Fe1-N3	2.252(9)	Fe1-N1	2.140(9)
Fe1-N2	2.290(10)		
Cl1-Fe1-Cl2	127.59(12)	N3-Fe1-Cl1	97.0(2)
N3-Fe1-Cl2	91.9(2)	N3-Fe1-N2	153.1(3)
N1-Fe1-Cl1	117.7(2)	N1-Fe1-Cl2	114.7(2)
N1-Fe1-N3	76.9(3)	N1-Fe1-N2	76.4(3)
N2-Fe1-Cl1	98.5(3)	N2 -Fe1 -Cl2	95.9(3)

Table S3. *Selected bond lengths (Å) and bond angles (°) for* ***1d****.*

Fe01-Cl1	2.4648(7)	Fe01-Cl1'	2.4923(7)
Fe01-Cl2	2.3192(7)	Fe01-O2	2.2048(16)
Fe01-N1	2.298(2)	Fe01-N2	2.289(2)
Cl1-Fe01-Cl1'	82.60(2)	Cl2-Fe01-Cl1'	99.24(2)
Cl2-Fe01-Cl1	103.17(2)	O2-Fe01-Cl1'	95.53(5)
O2-Fe01-Cl1	87.53(5)	O2-Fe01-Cl2	162.72(5)
O2-Fe01-N1	71.43(6)	O2-Fe01-N2	68.87(7)
N1-Fe01-Cl1	157.39(5)	N1-Fe01-Cl1'	91.09(5)
N1-Fe01-Cl2	99.26(5)	N2-Fe01-Cl1'	164.04(5)
N2-Fe01-Cl1	93.04(5)	N2-Fe01-Cl2	96.69(5)
N2-Fe01-N1	87.11(7)	Fe01-Cl1-Fe01'	97.40(2)

Table S4. *Reaction rate, obtained from the amount of benzoic acid (BA) formed with time, for the oxidative decarboxylation of iron(II)-BF complexes with dioxygen.*

Complex	Rate
1a	0.0084 mMh^{-1}
1b	0.028 mMh^{-1}
2a	0.037 mMh^{-1}
2b	0.12 mMh^{-1}

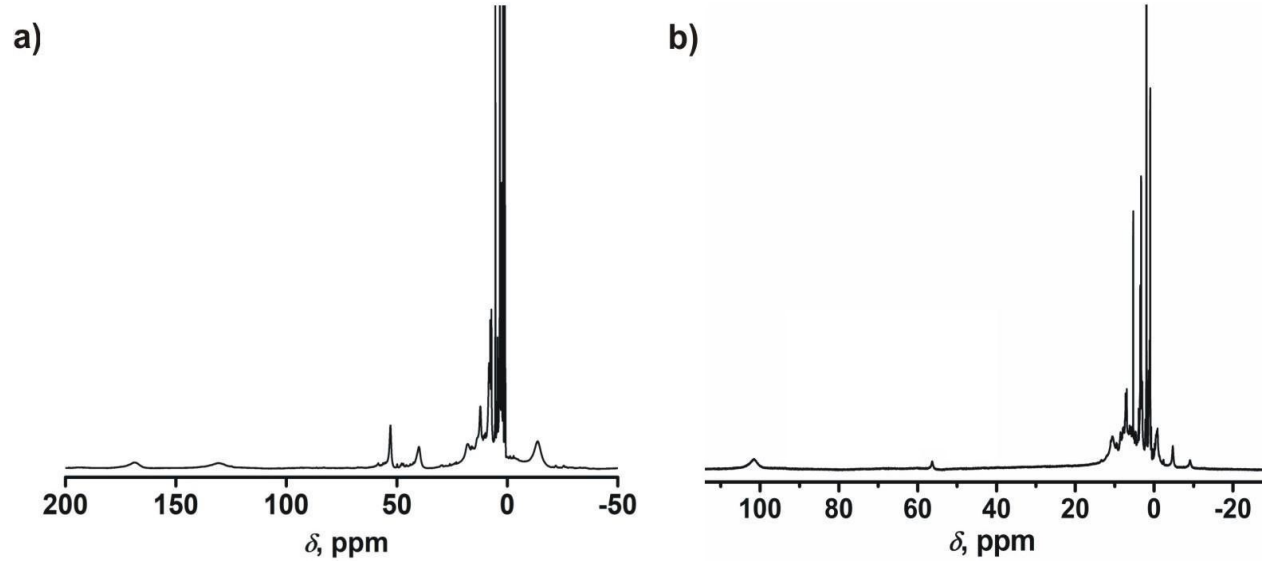

Figure S1. *^{1}H NMR (500 MHz, CD_3CN, 295 K) spectra of (a) [(6Me_2-Me-BPA)Fe(BF)](ClO_4) (**1a**) and (b) [(6Me_3-TPMM)Fe(BF)](ClO_4) (**1b**).*

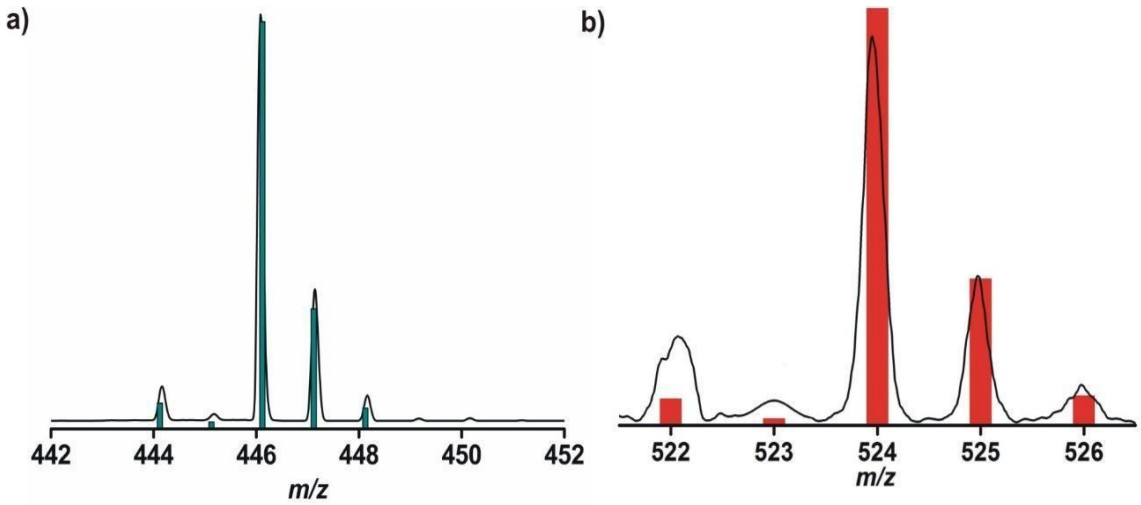

Figure S2. *ESI (positive ion mode in acetonitrile) mass spectra of (a) complex **1a** and (b) complex **1b**.*

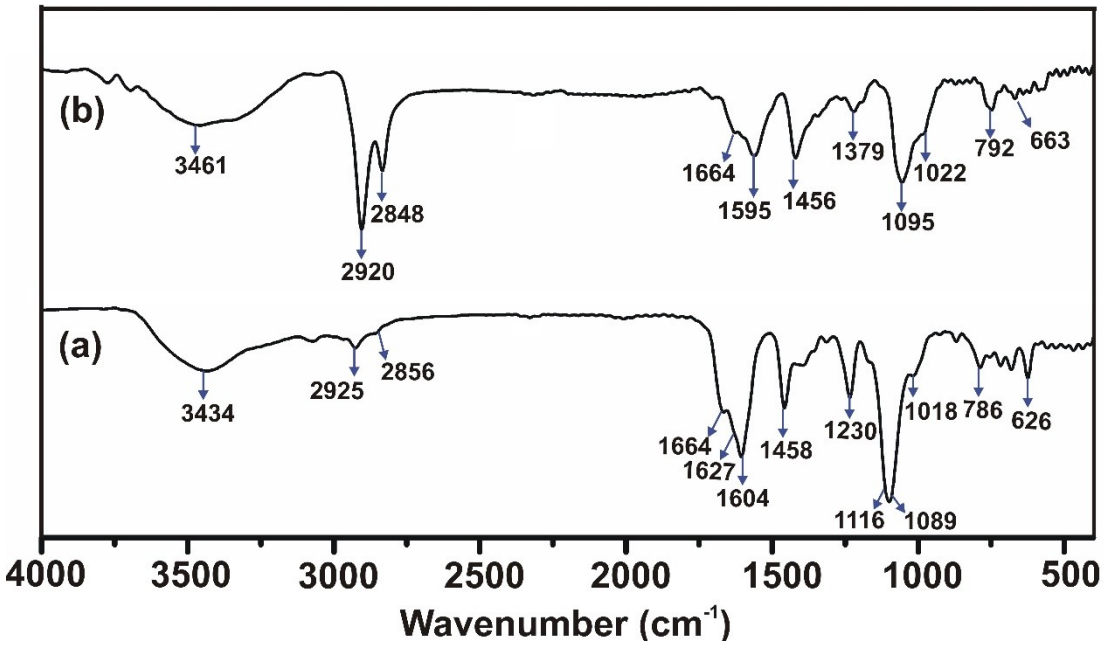

Figure S3. *Solid-state FTIR spectra of (a) complex* ***1a*** *and (b) complex* ***2a****.*

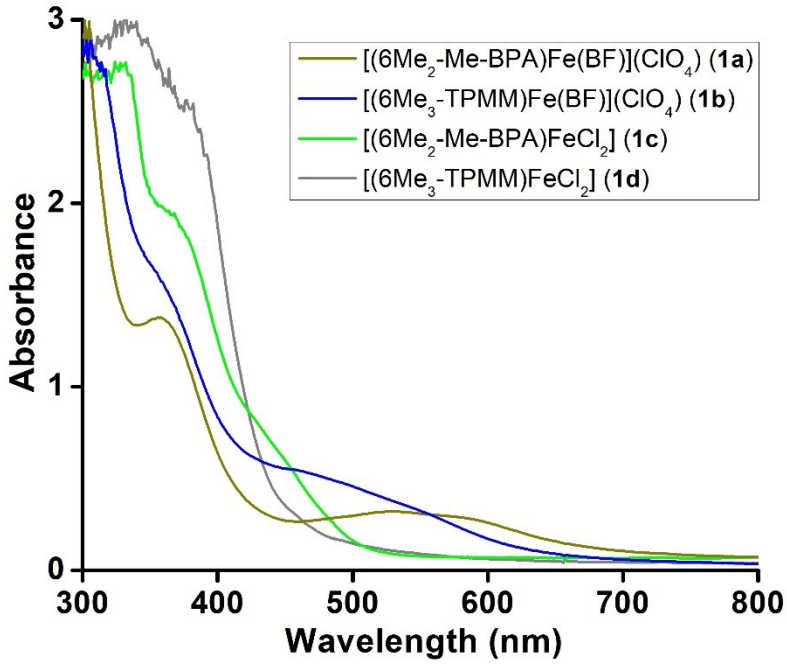

Figure S4*. UV-vis spectra of* ***1a****,* ***1b****,* ***1c*** *and* ***1d*** *in dichloromethane at 295 K.*

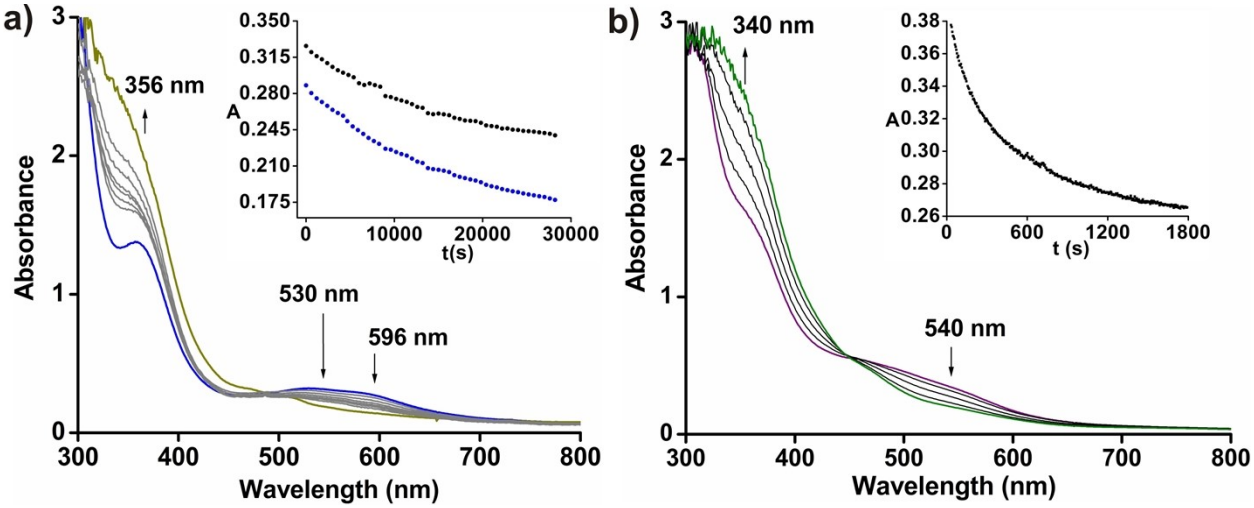

Figure S5. *Optical spectral changes during the reaction of (a)* ***1a*** *and (b)* ***1b*** *(1 mM) with dioxygen in dichloromethane at 295K. Insets: change of peak intensities as a function of time.*

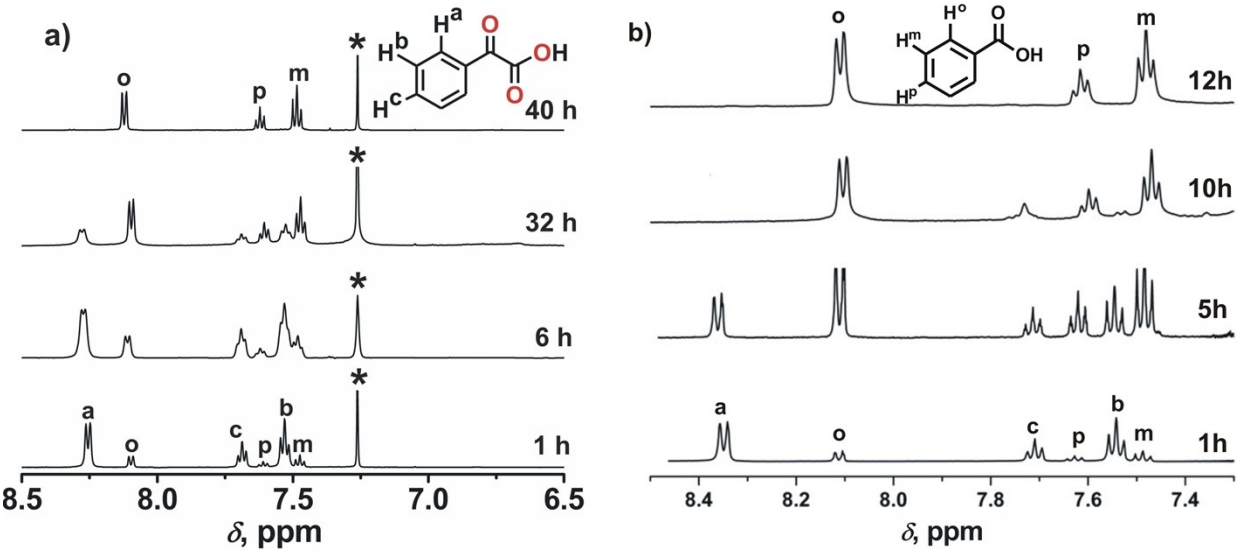

Figure S6. *Time-dependent ^{1}H NMR spectra (500 MHz, $CDCl_3$, 295 K) of the organic products formed during the reaction of (a)* ***1a*** *and (b)* ***1b*** *with dioxygen.*

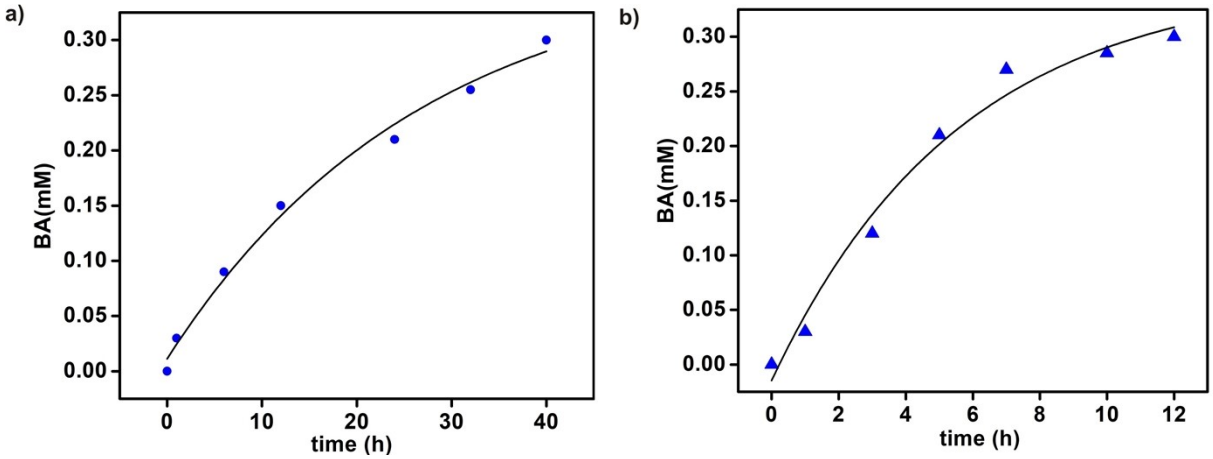

Figure S7. *Formation of benzoic acid (BA) as a function of time for the oxidative decarboxylation of (a)* ***1a*** *and (b)* ***1b****. Experimental condition: 0.003 mmol complex, 10 mL CH_3CN at 298 K.*

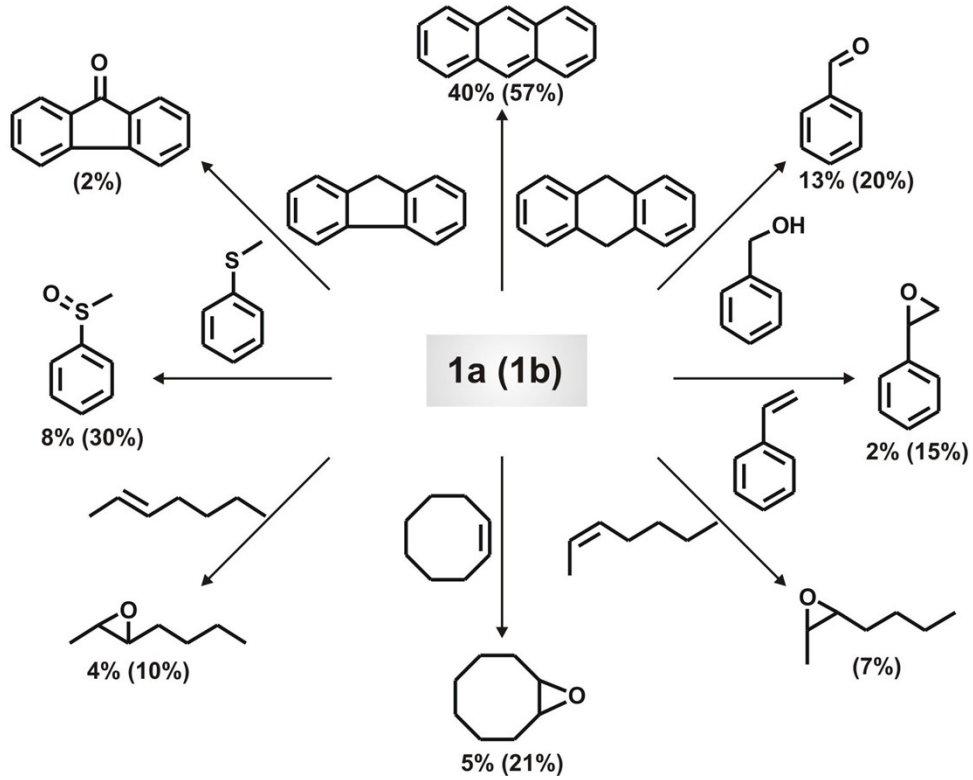

Scheme S1. *Interception of the iron-oxygen oxidant, formed from* ***1a (1b)*** *in the reaction with dioxygen, by external substrates.*

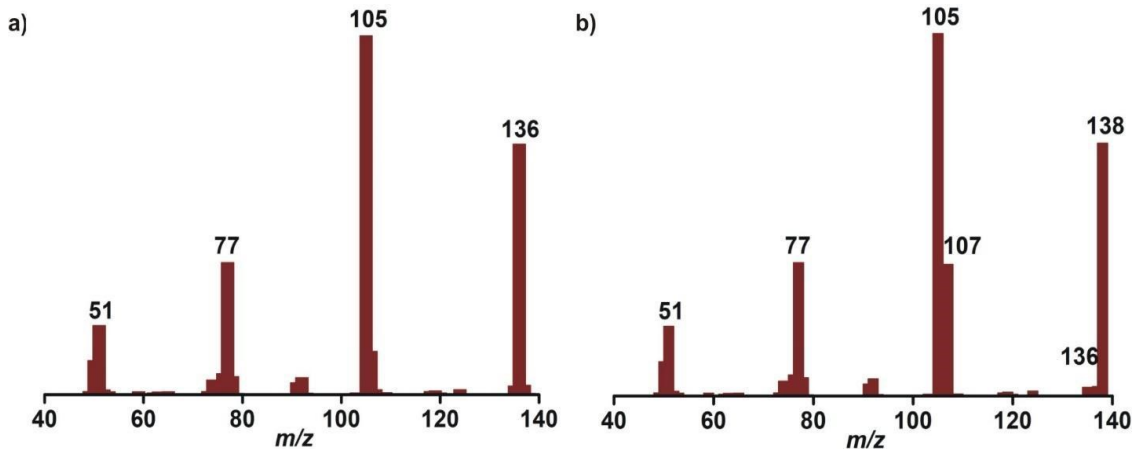

Figure S8. *GC-mass spectra of benzoic acid (as methyl ester) isolated from the reaction of* ***1a*** *with (a)* $^{16}O_2$ *and (b)* $^{18}O_2$.

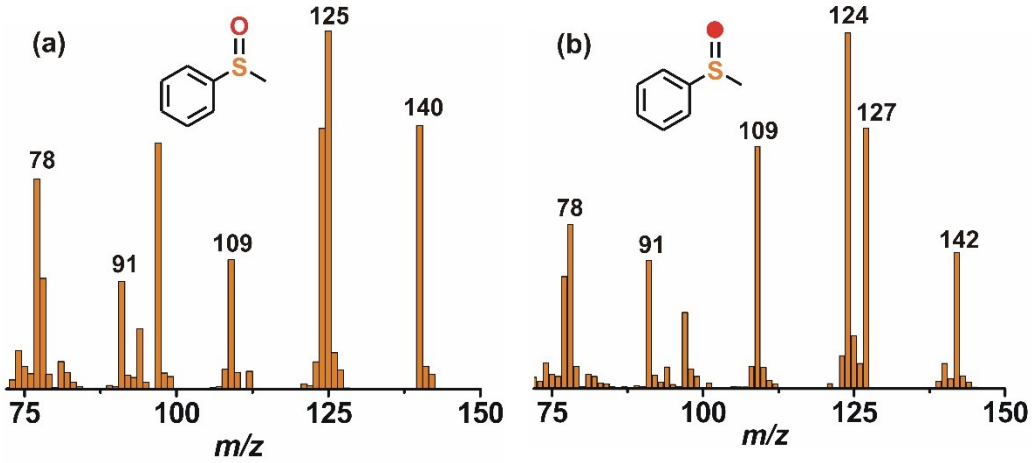

Figure S9. *GC-mass spectra of thioanisole oxide formed in the reaction of* ***1a*** *with thioanisole in the presence of (a)* $^{16}O_2$ *and (b)* $^{18}O_2$.

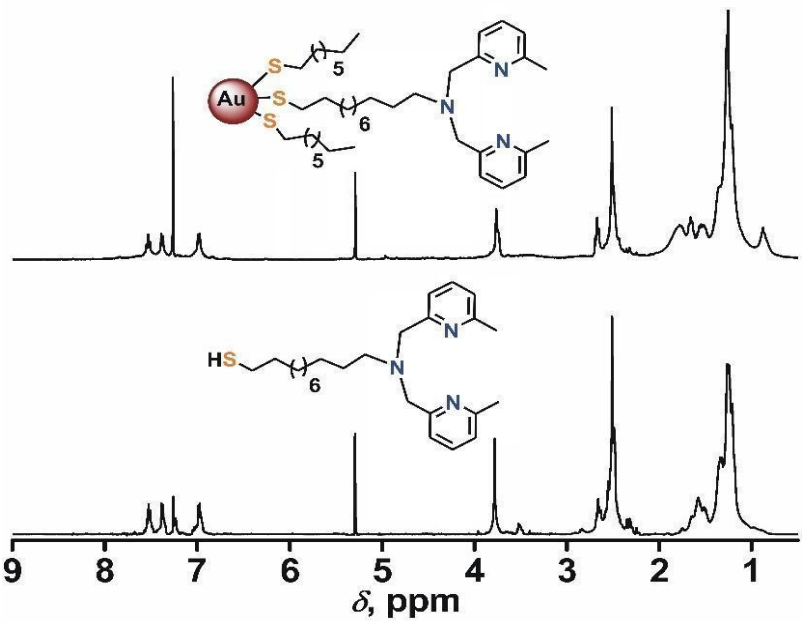

Figure S10. *^{1}H NMR spectra (500 MHz, $CDCl_3$, 295 K) of (a) $6Me_2$-BPASH and (b) ($6Me_2$-BPASH)@C_8Au.*

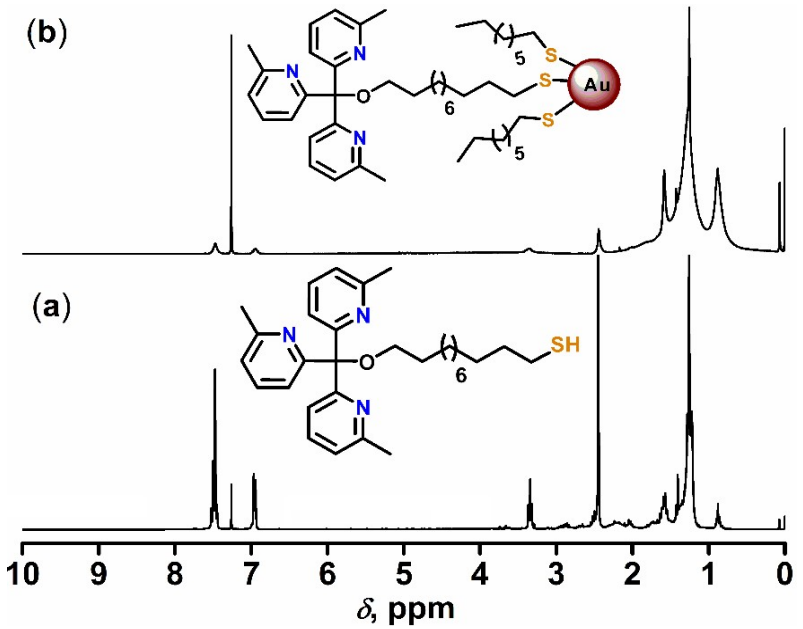

Figure S11. *^{1}H NMR spectra (500 MHz, $CDCl_3$, 295 K) of (a) $6Me_3$-TPMSH and (b) ($6Me_3$-TPMSH)@C_8Au.*

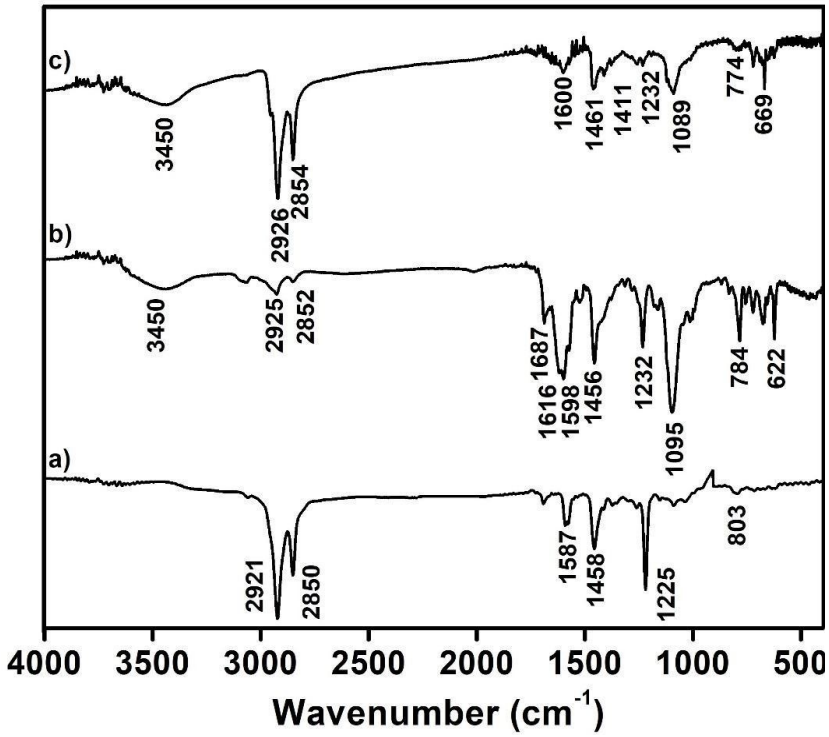

Figure S12. *FTIR spectra of (a) C_8Au, (b) complex* ***1b*** *and (c) complex* ***2b****.*

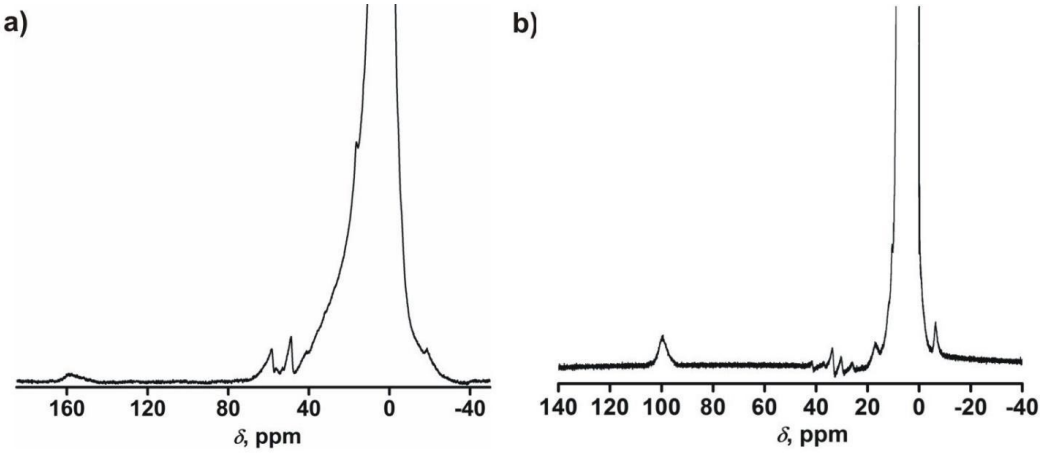

Figure S13. *^{1}H NMR (500 MHz, CD_3CN, 295 K) spectra of (a) complex* ***2a*** *and (b) complex* ***2b****.*

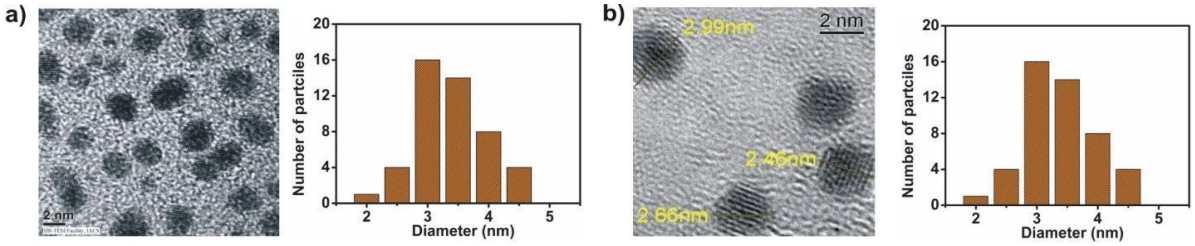

Figure S14. *TEM image (left) and histogram (right) for (a) complex* ***2a*** *and (b) complex* ***2b****.*

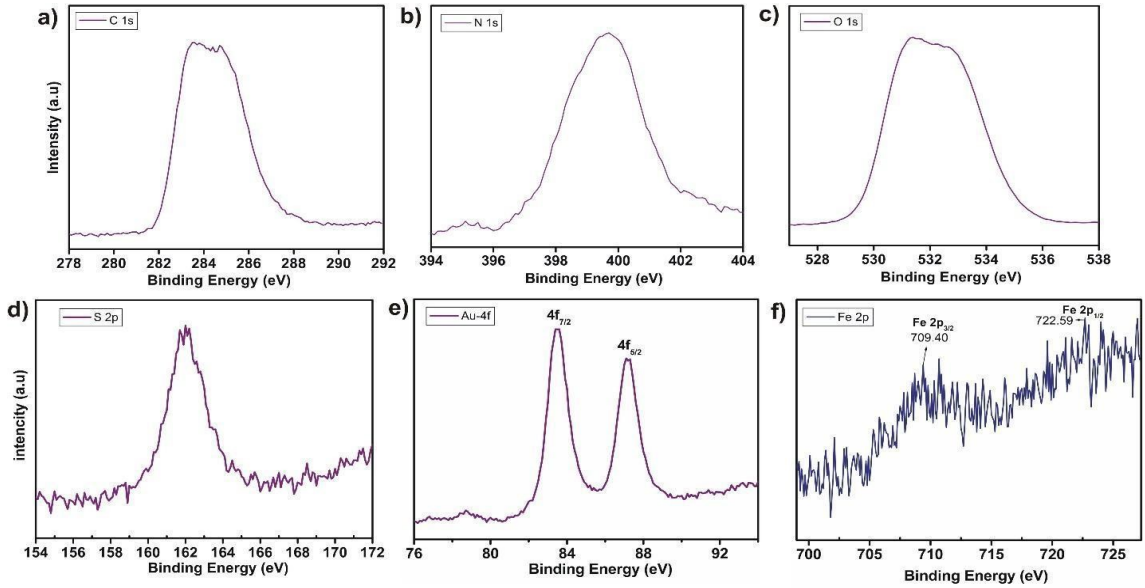

Figure S15. *XPS spectra of complex* ***2a****.*

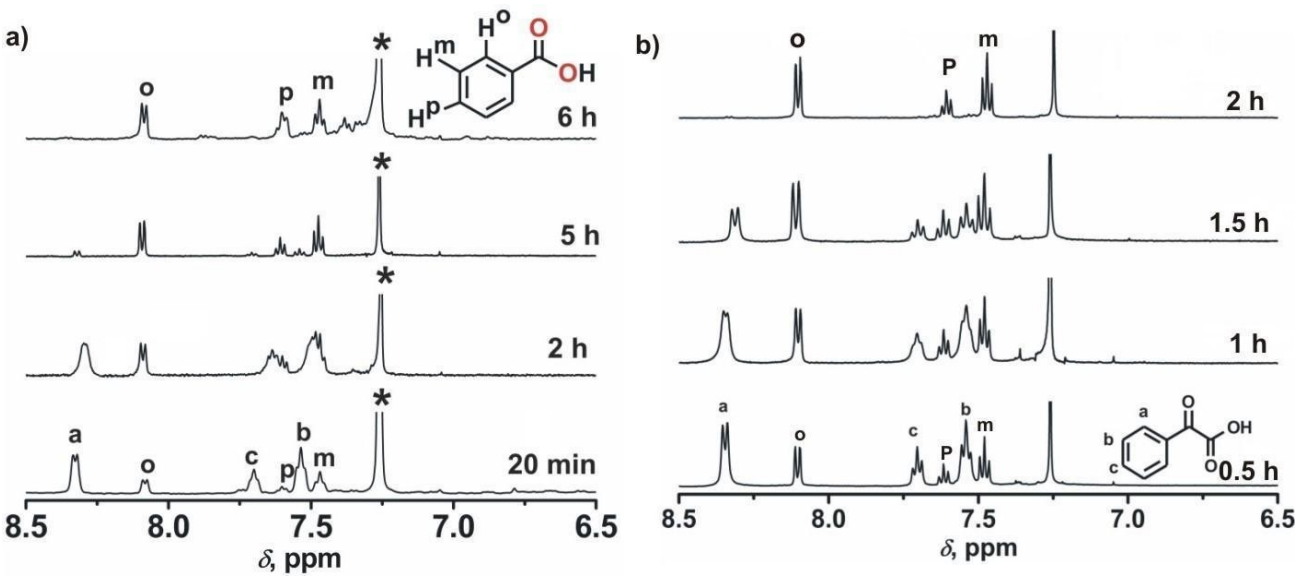

Figure S16. *Time-dependent ^{1}H NMR spectra (500 MHz, $CDCl_3$, 295 K) of the organic products formed during the reaction of (a) complex **2a** and (b) complex **2b** with dioxygen.*

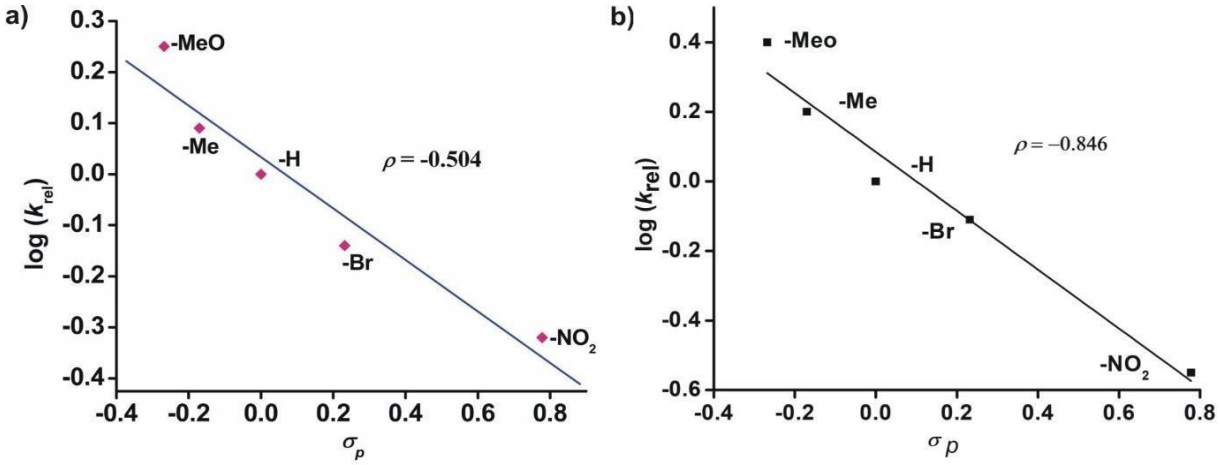

Figure S17. *Hammett plot of log k_{rel} against σ_p for para-substituted thioanisoles oxidation with complex **2a** and **2b**. The k_{rel} values are calculated by dividing the concentration of product from substituted thioanisoles by the concentration of product from thioanisole.*

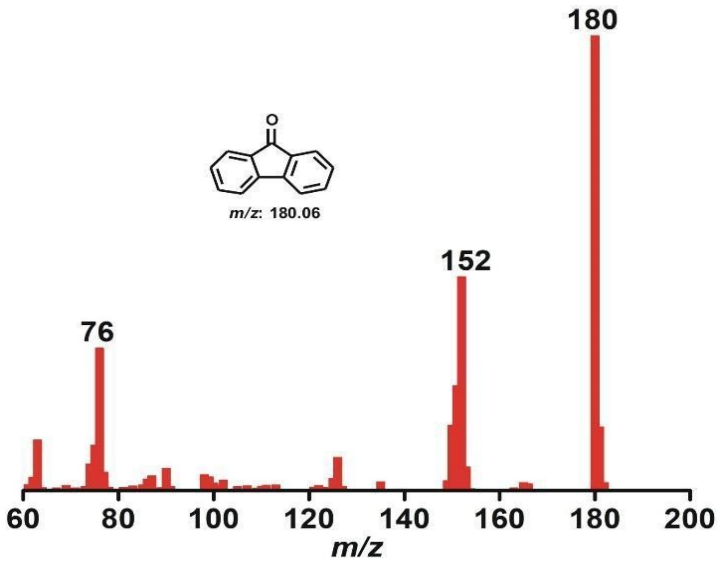

Figure S18. *GC-mass spectra of fluorenone formed from fluorene in the oxidation with complex* ***2b****.*

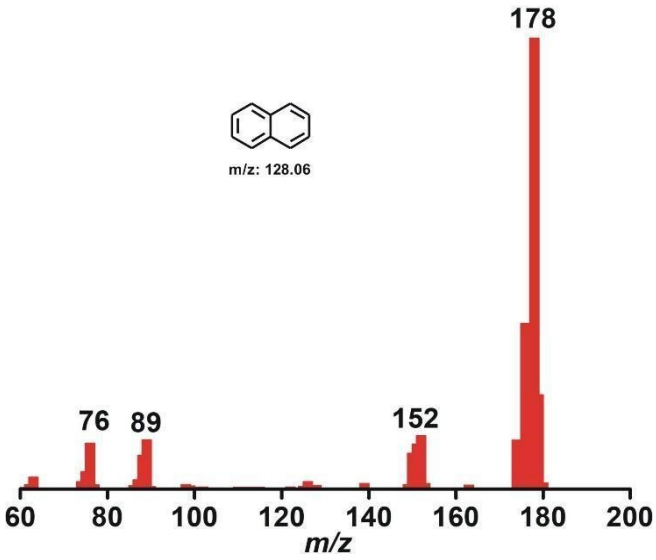

Figure S19. *GC-mass spectrum of anthracene formed from 9,10-dihydroanthracene in the oxidation with complex* ***2b****.*

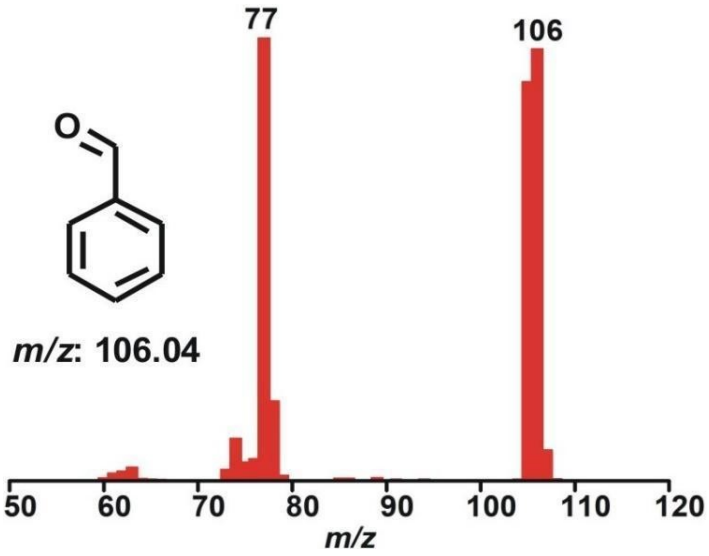

Figure S20. *GC-mass spectrum of benzaldehyde formed from benzyl alcohol in the oxidation with complex* ***2b****.*

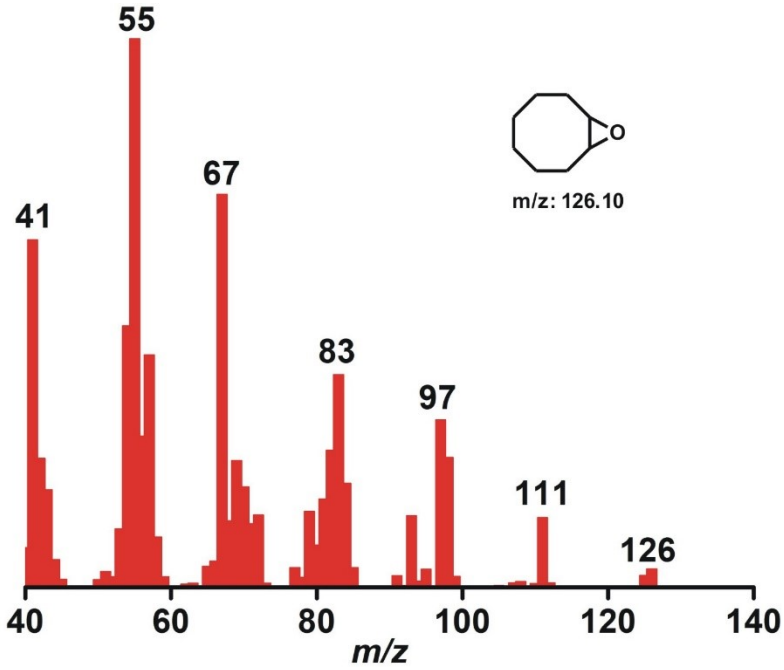

Figure S21. *GC-mass spectrum of cyclooctene epoxide formed from cyclooctene in the oxidation with complex* ***2b****.*

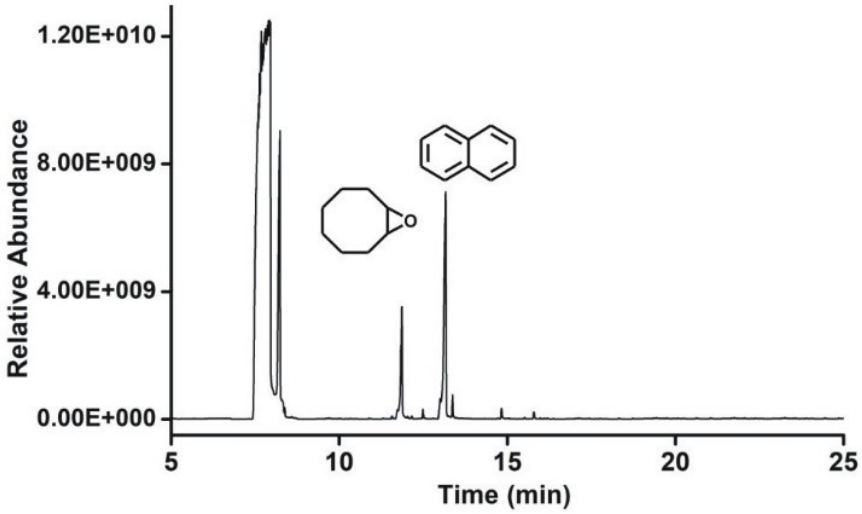

Figure S22. *Chromatogram of cyclooctene epoxide formed from cyclooctene in the oxidation with complex* ***2b****.*

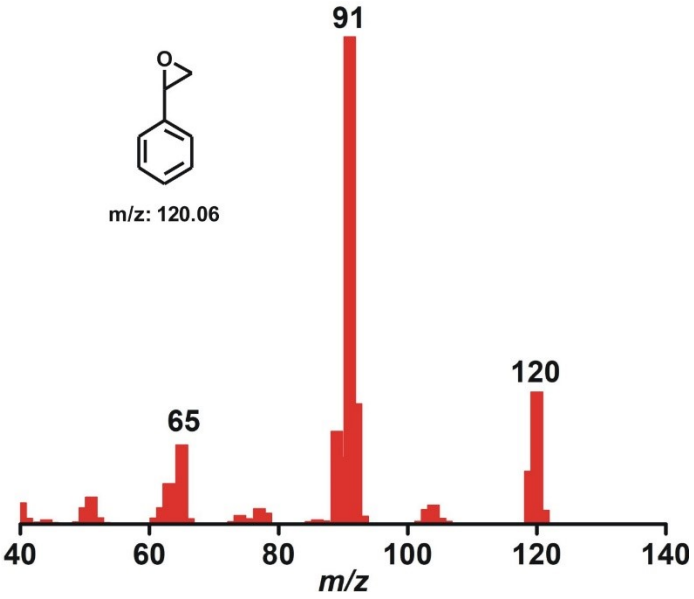

Figure S23. *GC-mass spectrum of styrene epoxide formed from styrene in the oxidation with complex* ***2b****.*

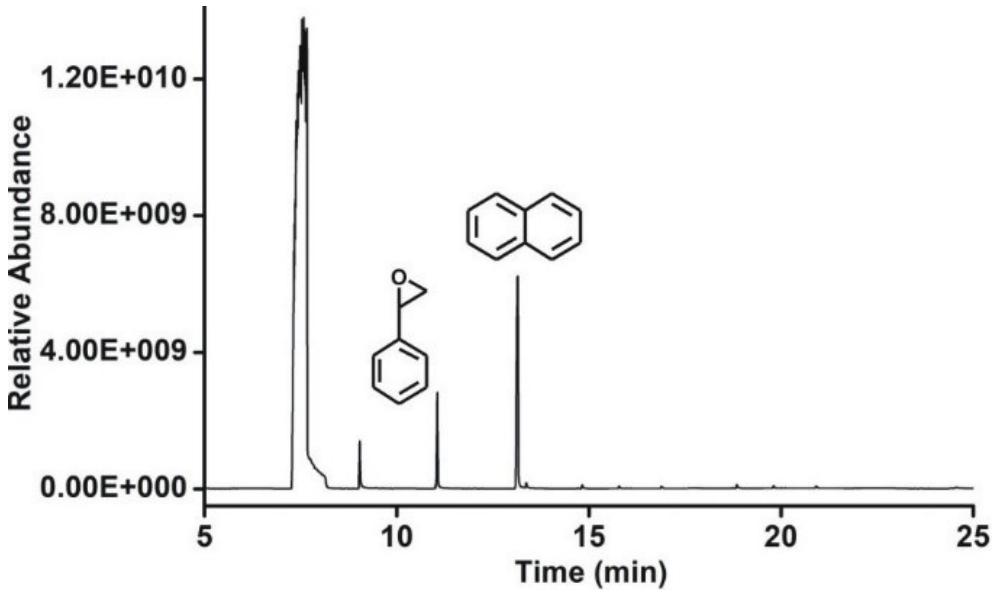

Figure S24. *Chromatogram of styrene epoxide formed from styrene in the oxidation with complex* ***2b****.*

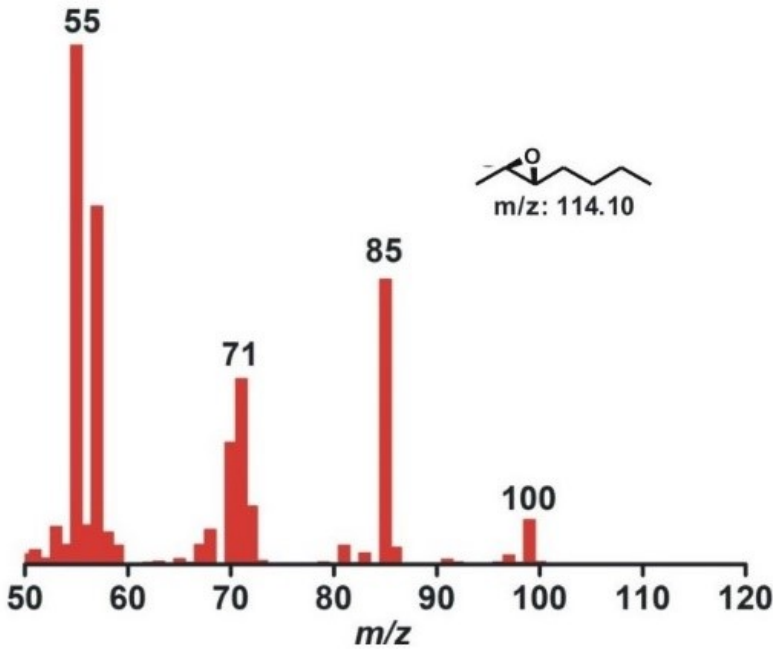

Figure S25. *GC-mass spectrum of trans-heptene epoxide formed from trans-2-heptene in the oxidation with complex* ***2b****.*

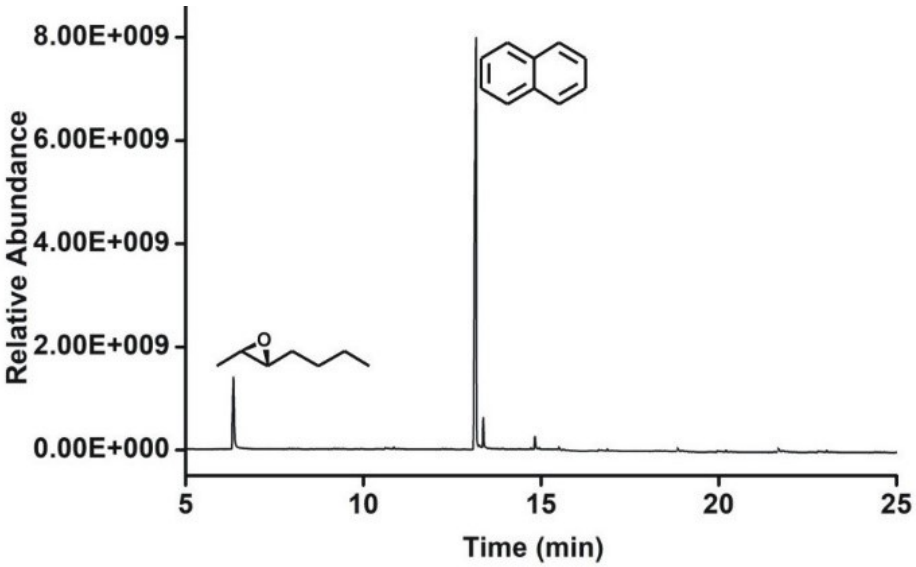

Figure S26. *Chromatogram of trans-heptene epoxide formed from trans-heptene in the oxidation with complex* ***2b****.*

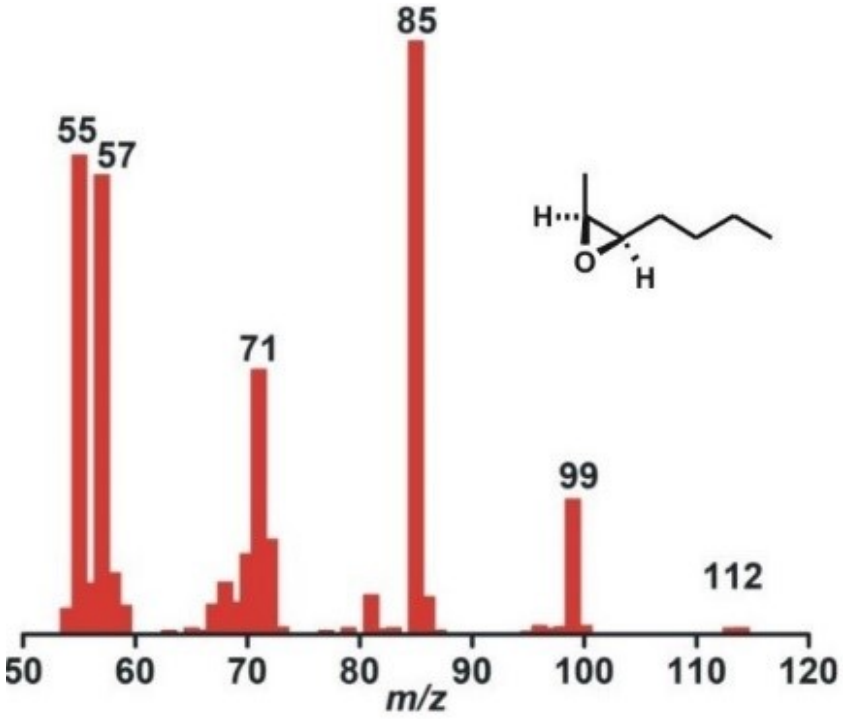

Figure S27. *GC-mass spectrum of cis-heptene epoxide formed from cis-2-heptene in the oxidation with complex* ***2b****.*

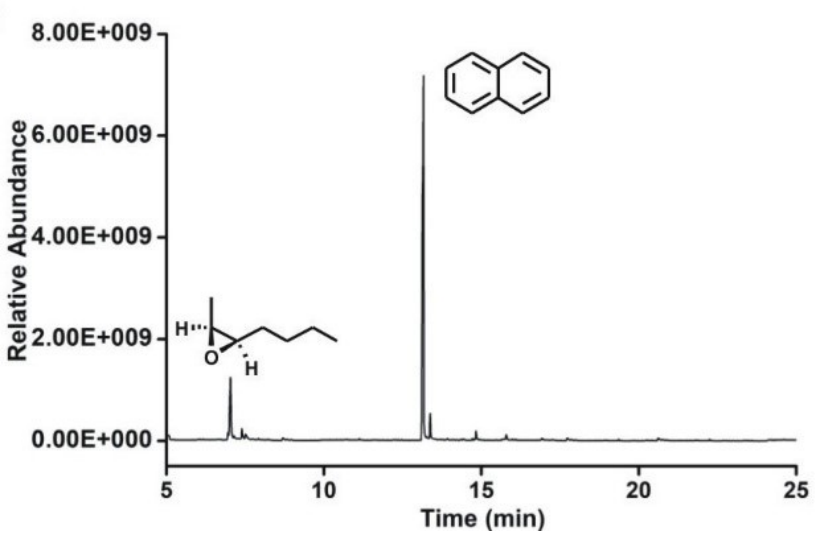

Figure S28. *Chromatogram of cis-heptene epoxide formed from cis-heptene in the oxidation with complex* ***2b****.*

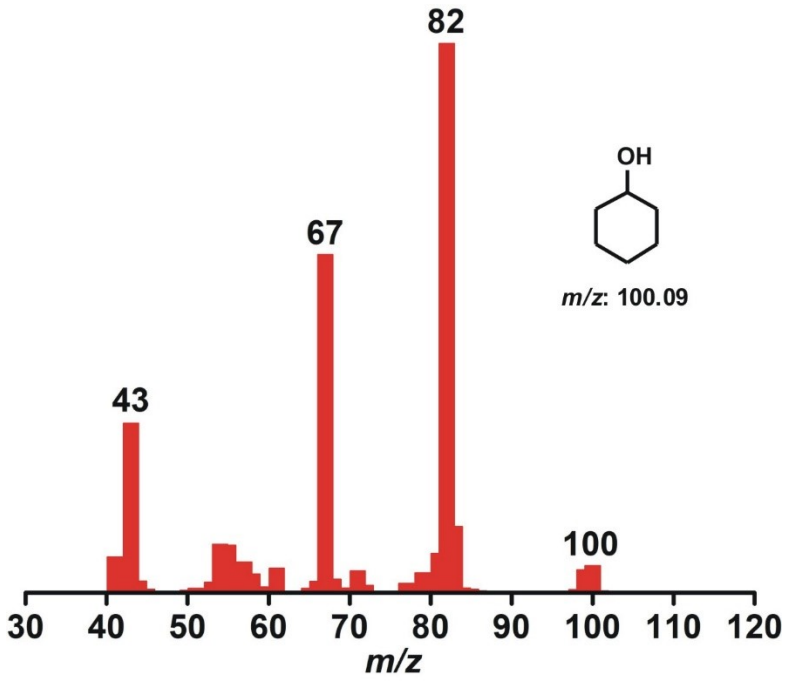

Figure S29. *GC-mass spectrum of cyclohexanol formed from cyclohexane in the oxidation with complex* ***2b****.*

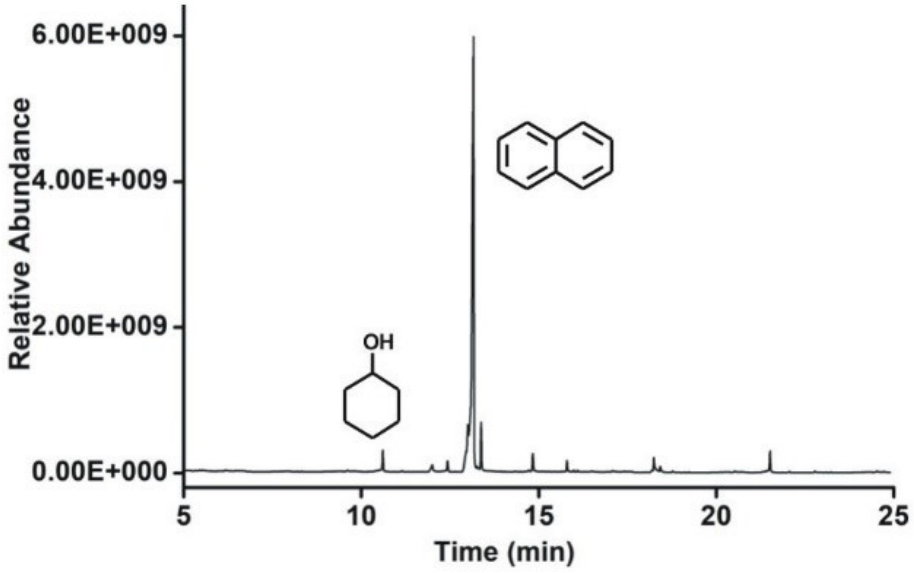

Figure S30. *Chromatogram of cyclohexanol formed from cyclohexane in the oxidation with complex* ***2b****.*

……..